This is a repository copy of *Design of annulene-within-an-annulene systems by the altanisation approach. A study of altan-[n]annulenes*.

White Rose Research Online URL for this paper:
http://eprints.whiterose.ac.uk/159005/

Version: Accepted Version

Article:
Piccardo, M., Soncini, A., Fowler, P.W. orcid.org/0000-0003-2106-1104 et al. (2 more authors) (2020) Design of annulene-within-an-annulene systems by the altanisation approach. A study of altan-[n]annulenes. Physical Chemistry Chemical Physics, 22 (10). pp. 5476-5486. ISSN 1463-9076

https://doi.org/10.1039/c9cp06835j

© 2020 Royal Society of Chemistry. This is an author-produced version of a paper subsequently published in Physical Chemistry Chemical Physics. Uploaded in accordance with the publisher's self-archiving policy.

Reuse
Items deposited in White Rose Research Online are protected by copyright, with all rights reserved unless indicated otherwise. They may be downloaded and/or printed for private study, or other acts as permitted by national copyright laws. The publisher or other rights holders may allow further reproduction and re-use of the full text version. This is indicated by the licence information on the White Rose Research Online record for the item.

Takedown
If you consider content in White Rose Research Online to be in breach of UK law, please notify us by emailing eprints@whiterose.ac.uk including the URL of the record and the reason for the withdrawal request.

eprints@whiterose.ac.uk
https://eprints.whiterose.ac.uk/

Journal Name

ARTICLE TYPE

Cite this: DOI: 00.0000/xxxxxxxxxx

Design of annulene-within-an-annulene systems by the altanisation approach. A study of *altan*-[n]annulenes

Matteo Piccardo,[a] Alessandro Soncini,*[a] Patrick W. Fowler,[b] Guglielmo Monaco,*[c] and Riccardo Zanasi[c‡]

Received Date
Accepted Date

DOI: 00.0000/xxxxxxxxxx

The altanisation strategy, devised to design molecules with large and paratropic perimeter circulations, is applied to the family of [*n*]annulenes to give $[2n,5]$coronenes. Analytical expressions are obtained for the eigenvalues of the Hückel Hamiltonian for *altan*-[*n*]annulenes, and used in conjunction with selection rules derived from the ipsocentric approach to predict patterns of global ring current in these systems. Density-functional calculations performed on seven *altan*-[*n*]annulenes, three neutral and four charged, give current-density maps in essential agreement with the predictions obtained at the unperturbed Hückel level. All but one of the systems show patterns with the tropicities expected for isolated annulenes, in line with the altanisation concept. The apparent exception is *altan*-[11]annulene$^-$, the only singlet system with a well defined open-shell character in the studied set. The key role of open-shell character can be accommodated by appropriate choice of the occupation numbers of the initial Hückel molecular orbitals, where the anion *altan*-[11]annulene$^-$ is considered as an [11]annulene inside the [22]annulene anion.

1 Introduction

In the search for new stable molecules as possible candidates for development of electronic devices, particular attention has been paid to antiaromatic molecules.[1–4] Designs based on introduction of a cyclooctatetraene ring,[2] pentalene units,[3] or structures with $4N$ conjugated π electrons in stripes of pentagonal and benzenoid rings[4] have all been discussed. A different approach starts from the finding that the induced current density computed for $[2n,5]$coronenes[5,6] is consistent with the annulene-within-an-annulene model,[7,8] even though this is generally a poor model for most coronenes.[9–16] This unusual behavior is understood considering that all bonds linking the two annulenes (the spokes) are fixed single bonds, and this typically determines the onset of isolated patterns in the full whole current-density map.[17] In such a case, counting carbon atoms is sufficient to anticipate the tropicity of the annulenes, and this expectation can be used to design closed-shell molecules where the perimeter current loop has sufficient area to lead to an overall average paramagnetic response for the whole molecule.[6]

Further insight into the unusual behaviour of $[2n,5]$coronenes is obtained by inspection of molecular orbitals. Considering the perimeter as a starting fragment, it can be seen that one of its degenerate frontier orbitals does not have the correct nodal structure to couple with the π orbitals of the inner annulene (the hub).[5,6,18] Thus, the degenerate pair splits on connecting the two annulenes, and a paratropic circulation on the perimeter can be predicted according to the ipsocentric approach[19,20] (this kind of symmetry-breaking differs from the one considered in the pioneering study on paramagnetic ring currents[21], as it is based on alteration of diagonal, rather than extradiagonal, elements of the adjacency matrix). $[2n,5]$coronenes were recognized as particular cases of the class of *altan*-molecules,[18,22–26] constructed from parent molecules by the formal topological operation that transforms a parent $[2n]$annulene into a $[2n,5]$coronene. This operation, later called altanisation,[25] consists in the replacement of the *exo* C–H bonds of the parent molecule by C–C bonds to *alt*ernate three-cooordinate C atoms of an outer *an*nulene perimeter. Altanisation as a topological operation was formalized by Gutman, considering any subset of C-H bonds.[24,27] $[2n,5]$coronenes are equivalent to *altan*-[$2n$]annulenes, and we will adopt this terminology in the following.

A simply connected (totally fused) Kekulean molecule has no *endo* C-H bonds and has an even number of *exo* C-H bonds (see note 9 of ref.[28]). When altanisation is performed on such a molecule, the unique perimeter has $4N$ π electrons and is

[a] School of Chemistry, University of Melbourne, Victoria, 3010, Australia; E-mail:asoncini@unimelb.edu.au.
[b] Department of Chemistry, The University of Sheffield, Sheffield S3 7HF, United Kingdom
[c] Department of Chemistry and Biology, University of Salerno, Fisciano 84084, Italy; E-mail:gmonaco@unisa.it

expected to hold a paratropic current.

Computational tests of the effectiveness of the altanisation strategy have been generally positive.[18,23,25,26,29] Exceptions are the diatropic perimeters reported for *altan*-kekulene[18,23] and *altan*^{2}-[10]annulene.[25,28] These molecules, which appear at the bottom of the list of studied annulenes, when sorted for the ratio of the perimeters of the altan and its parent molecule (their ratios being 1.20 and 1),[26] are predicted to be open-shell singlets.[28] Beyond antiaromatic species, molecules with an open-shell singlet ground state are also attracting attention as candidates for organic electronic devices.[30] Altanisation may be a versatile strategy in the quest of efficient new materials.

Recently, the first two *altan*-molecules have been synthesized.[31,32] These stable cyclopenta-ring-fused oligo(*m*-phenylene) macrocycles, which have been named 8MC and 10MC on the basis of the number of five or six membered rings present in the macrocycle, can be recognized as the *altans* of two annulenes, that are not themselves in an all-*cis* conformation. Using the IUPAC recommended abbreviations T and C for *cis* and *trans*,[33] the conformation of the hub of 8MC can be recognized as $(CTT)_8$; thus, 8MC is *altan*-$(CTT)_8$[24]annulene and, similarly, 10MC is *altan*-$(CTT)_{10}$[30]annulene (Figure 1). The presence of T configurations of double bonds in the parent annulene leads to *altan*-derivatives that have belts of alternating hexagons and pentagons, thus releasing the strain expected for *altans* of all-*cis* annulenes. For both molecules, the paratropic loops that would be predicted on the basis of simple C atom counting (hub and rim in 8MC, and rim in 10MC) turn out to be diatropic instead. As with the two failures of the altanisation prediction found by calculations,[26,28] the ground states of 8MC and 10MC are open shells. Interestingly, 8MC and 10MC can still be considered as formed from decoupled annulenes, but with one or both in the triplet state and thus hosting a diatropic current, consistently with Baird's rule of aromaticity.[34,35] However interpreted, it is a matter of fact that the only two *altan*-molecules synthesized so far have a diatropic perimeter, pointing to the case for revisiting the design strategy. To investigate further, we decided to study altans of charged annulenes with a $4N+2$ perimeter, which can be expected to host a diatropic current, if the two annulenes are fully decoupled. We focused on *altan*-[9]annulene$^{\pm1}$ and *altan*-[11]annulene$^{\pm1}$, which bracket the hub size in planar *altan*-[10]annulene ([10,5]coronene[5,36]). In these charged systems, the spokes are not fixed single bonds, so the assumption of a decoupled perimeter fails, as it would in a neutral *altan*-molecule, if a double bond is allowed to un-pair to account for the open-shell singlet character. Taking *altan*-[11]annulene as an example (Fig. 2), there are 11×2 resonance structures with single bonds on all spokes (and a hub-localised charge) and 11^2 resonance structures with one double-bond spoke and the charge localized on the rim. An 8-electron circuit can be easily recognized in resonance structures such as a11a-II, and competition between diatropic and paratropic circulations on the rim can be anticipated.[37,38] In general, there are $n/2$ times as many structures with the charge on the rim as there are with the charge on the hub, and thus their influence can be expected to grow with the dimension of the parent annulene.

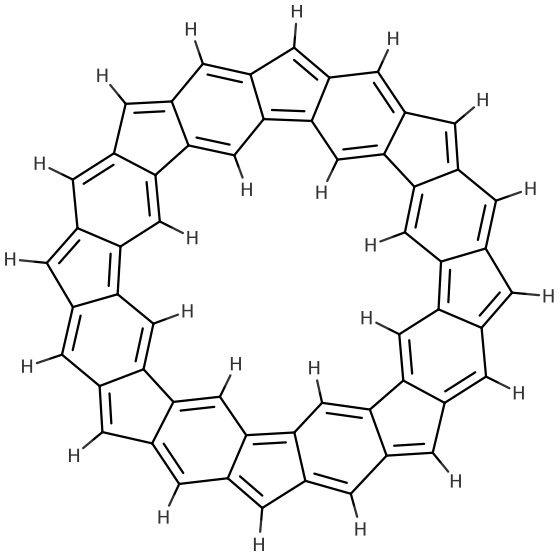

Fig. 1 Structure of the synthesized *altan*-$(CTT)_8$[24]annulene.

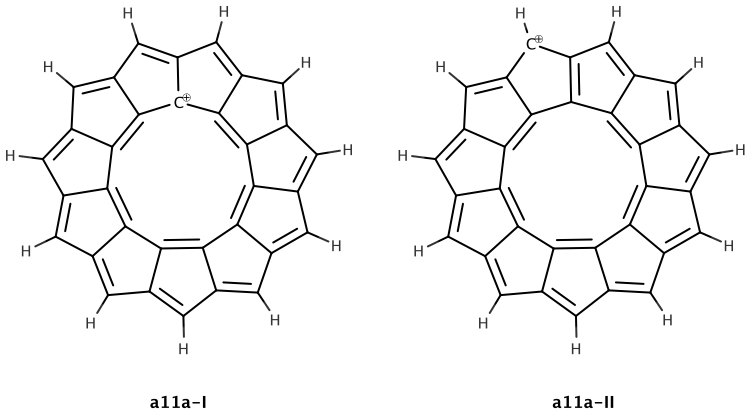

Fig. 2 Limiting resonance forms of an ion *altan*-[11]annulene. Form I has all spokes as single bonds, and form II has a double bond on one spoke. A 4*N* (8) π-electron circuit occurs in form II.

This investigation of an altanisation strategy gives us the opportunity to consider the systematics of the whole class of *altan*-[*n*]annulenes, for even and odd *n*. In the following, we review the model for predicting the tropicity of a transition within the ipsocentric approach,[19,20] link it to the systematics of the eigenvalues of *altan*-[*n*]annulenes within the tight-binding approach and the consequences for the selection rules that determine overall appearance of their ring-current patterns, and, finally, we confront these considerations with full *ab initio* calculations for charged and neutral *altan*-[*n*]annulenes. Open-shell character is shown to be a key factor for the nature of the perimeter currents in altans.

2 Ipsocentric predictions

According to the ipsocentric Ansatz for solution[19,39–41] of the gauge problem, the current-density induced by an external magnetic field is a sum of contributions from virtual transitions allowed under linear- and angular-momentum selection rules.[42] Transitions are between occupied and empty orbitals. Consideration of a small number of transitions between orbitals close to the Fermi level is generally sufficient to predict the sense of the current,[43] often in a near-quantitative manner. The linear-momentum (translational) transitions give diatropic contributions, and the angular-momentum (rotational) transitions give mainly[44] paratropic contributions. Although the ipsocentric method is not restricted to the tight binding level, it is known that for conjugated hydrocarbons, currents obtained at this level are often sufficient to give the same global tropicities obtained ab initio.[45] The simplest predictions require the determination of energy levels and identification of the character of transitions between orbitals close to the Fermi level. Identification of the nature of the transitions is simplified in cases where the system has non-trivial point-group symmetry. In that case the consideration of the azimuthal node-count is particularly helpful.

For regular [*n*]annulenes, with a C_n symmetry axis, orbitals can be labelled by a quantum number which, following a suggestion by Mulliken, has been called *orbital ring quantum number* q,[46] or quasi-angular momentum m,[47–49] or angular momentum (k[20] or λ[43,50]) for short. The value of q can be inferred from the Mulliken symbol (for C_n groups, representations A, B and E_q have ring quantum number 0, $n/2$ and q), or by inspection, since its modulus $|q|$ is equal to half the azimuthal node count (HANC).[22] Character tables show that rotationally and translationally allowed transitions are characterized by $\Delta q = 0$ and $\Delta q = \pm 1$, respectively.[20] Consideration of the frontier orbitals then predicts diatropic/paratropic currents for $4N+2/4N$ singlet annulenes,[20] and paratropic/diatropic currents for $4N+2/4N$ triplet annulenes.[51]

Upon lowering the C_n symmetry, q is no longer a proper quantum number, but the HANCs change slowly, so that identification of translationally or rotationally allowed transitions as those with $\Delta(\text{HANC}) = 0$ or ± 1 is often successful. In particular, for *altan*-[*n*]annulenes the maximum order for a rotation axis is n, and thus, even in the highest possible symmetry, q cannot exceed $n/2$. However, if the distortion of the outer annulene by the inner is sufficiently small, orbitals of the isolated outer annulene with $q > n/2$ can preserve HANC $> n/2$ even in the *altan*-[*n*]annulene, and the $\Delta(\text{HANC}) = 0, \pm 1$ rule can still be used as a guide to the character of the transition. We label the orbitals of *altan*-[*n*]annulenes ($\text{HANC}_{\text{hub}} \pm \text{HANC}_{\text{rim}}$), depending on whether the hub and rim orbitals are in- or out-of-phase. HANC labelling can then be used to predict diatropic currents for hub ($\Delta(\text{HANC}_{\text{hub}}) = \pm 1$) or rim ($\Delta(\text{HANC}_{\text{rim}}) = \pm 1$) stemming from translationally allowed transitions. For rotationally allowed transitions the HANC changes on the two annulenes are insufficient and the relative sign of orbitals on hub and rim is needed: for a transition with $\Delta(\text{HANC}_{\text{hub}}) = \Delta(\text{HANC}_{\text{rim}}) = 0$ and in- or out-of-phase combinations of the annulenic orbitals in both occupied and virtual orbitals, two paratropic circulations are expected, but if the occupied orbital is an in-phase and the virtual orbital an out-of-phase combination (or vice-versa), the current on the hub will be diatropic.[44,52] In contrast with [*n*]circulenes, no pairs with combinations of opposing phase are found in *altan*-[*n*]annulenes, and rotationally allowed transitions between Jahn-Teller-split descendants of degenerate pairs are therefore expected to give paratropic currents on both hub and rim.

The ipsocentric prediction of a paratropic perimeter for *altan*-molecules is based on the assumption of small coupling of annulene orbitals with the orbitals of the hub. If the coupling is strong enough, one can expect other orbitals to intrude between the splitting pair and introduce translationally-allowed transitions, so that the prediction is reversed. This intrusion has been verified in the case of *altan*-kekulene and *altan*^{2}-[10]annulene.[28]

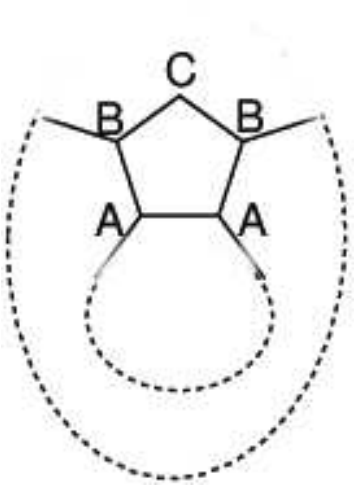

Fig. 3 Type of carbon atoms in an *altan*-[*n*]annulene.

3 Tight-binding Energy Levels

An *altan*-[*n*]annulene in C_n symmetry has three symmetry-unique C atoms (Figure 3): one (C^A)) in the hub, and two (C^B and C^C) on the rim; C^B is connected to three C atoms and C^C is connected to two C atoms. For each such atom, e.g. C^A, the n atomic orbitals (χ_1^A, $\chi_2^A \ldots \chi_n^A$ for C^A), can be used to form n symmetry-adapted linear combinations ($\psi_q^A = \sum_j c_{jq} \chi_j^A$), with complex coefficients

$$c_{jq} = \frac{1}{\sqrt{n}} \sum_{j=0}^{n-1} \exp\left(\frac{2\pi i j q}{n}\right), \qquad (1)$$

with $j = 0, 1, \ldots n-1$ counting atoms, and $q = 0, \pm 1, \pm 2 \ldots \pm(\frac{n}{2} - 1), \frac{n}{2}$ the ring quantum number (where $n/2$ is allowed only for even n). Symmetry allows mixing of orbitals of equal q only, and this implies that the Hückel Hamiltonian for an *altan*-[n]annulene is block-diagonal, with 3×3 blocks for each q. In order to investigate the interpretation of *altan* wavefunctions in terms of annulene wavefunctions, rather than symmetry-adapted linear combinations, it is expedient to write the Hückel Hamiltonian as

$$\widehat{H} = \widehat{H}_{\rm rim} + \widehat{H}_{\rm hub} + \widehat{H}_{\rm spoke},$$

and take as basis functions the solutions in the absence of $\widehat{H}_{\rm spoke}$, *i.e.,* the eigenfunctions of independent [n] and [$2n$]annulenes ($\psi_q^{\rm hub}$ and $\psi_q^{\rm rim}$), where the coefficients are given by equation (1) and the eigenvalues are $\varepsilon_q = 2\cos(2\pi q/n)$, for the [$n$]annulene, and by the same function with n replaced by $2n$ for the [$2n$]annulene. Ring quantum numbers on hub and rim will be denoted q and q', respectively.

The coupling elements between annulenes are then

$$\left\langle \psi_{q'}^{\rm rim} \middle| \widehat{H}_{\rm spokes} \middle| \psi_q^{\rm hub} \right\rangle = \frac{\beta}{n\sqrt{2}} \sum_j \exp\left[\frac{2\pi i j (q'-q)}{n}\right] = \quad (2)$$

$$= \frac{\beta}{n\sqrt{2}} \frac{1-\exp\left[2\pi i j (q'-q)\right]}{1-\exp\left[\frac{2\pi i j (q'-q)}{n}\right]}, \quad (3)$$

which vanish unless $q' - q = \pm kn$, with k an integer, when they are $\beta/\sqrt{2}$. This implies that ψ_q is coupled with $\psi_q^{\rm rim}$ and $\psi_{n-q}^{\rm rim}$ only. The two q values for the rim can be understood as stemming from in- or out-of-phase combinations of the symmetry-adapted linear combinations on the degree-3 and degree-2 rim C atoms:

$$\psi_{q'}^{\rm rim} = \frac{1}{\sqrt{2}} \psi_{q,3}^{\rm rim} \pm \frac{1}{\sqrt{2}} \psi_{q,2}^{\rm rim}.$$

Here the plus sign corresponds to $q' = q$ and the minus sign to $q' = n - q$. The 3×3 block of the Hückel Hamiltonian on the subset $\left(\psi_q^{\rm rim}, \psi_{n-q}^{\rm rim}, \psi_q^{\rm hub}\right)$ is therefore

$$H_q = \begin{bmatrix} 2\cos(\frac{\pi q}{n}) & 0 & \frac{1}{\sqrt{2}} \\ 0 & -2\cos(\frac{\pi q}{n}) & \frac{1}{\sqrt{2}} \\ \frac{1}{\sqrt{2}} & \frac{1}{\sqrt{2}} & 2\cos(\frac{2\pi q}{n}) \end{bmatrix}.$$

The eigenvalues of the above matrix satisfy the following cubic equation,

$$x^3 - 2\cos\left(\frac{2\pi q}{n}\right) x^2 - \left(4\cos^2\left(\frac{\pi q}{n}\right) + 1\right) x + 8\cos^2\left(\frac{\pi q}{n}\right) \cos\left(\frac{2\pi q}{n}\right) = 0, \quad (4)$$

which can be written

$$x^3 - \varepsilon_q x^2 - (\varepsilon_q + 3)\, x + \varepsilon_q^2 + 2\varepsilon_q = 0. \quad (5)$$

Eq. (4) provides the link between the energies and q-symmetry of the parent [n]-annulene: each q for the parent generates three states of the derived *altan*-[n]annulene. The spectrum of the *altan* is therefore the sum of three (distorted) copies of the annulene spectrum. Several properties of the *altan*-[n]annulene spectrum can be derived immediately on the basis of Eq. (5) :

1. Every degenerate eigenvalue of the [n]annulene corresponds to $+q$ and $-q$ partners. Since Eq. (4) depends on cosine functions of q only, it follows that each degenerate level produces three doubly degenerate levels in the *altan*-[n]annulene spectrum.
2. Every *even* annulene has top eigenvalue $\varepsilon_{n/2} = -2$, so that the final coefficient in the cubic (5) vanishes and we obtain $x_{n/2}\left(x_{n/2}^2 + 2x_{n/2} - 1\right) = 0$. Hence, every *altan*-[$n$]annulene derived from an even annulene has at least one non-bonding orbital $x_{n/2} = 0$, one bonding level $x_{n/2} = 1 + \sqrt{2}$, and an antibonding level $x_{n/2} = 1 - \sqrt{2}$. The zero is always associated with a $q = n/2$ orbital that has nonzero weights on alternating atoms of the rim.
3. If the parent [n]-annulene has an antiaromatic count ($n = 4N$, $N = 1, 2 \ldots$), its spectrum contains two non-bonding levels with angular momentum $q = n/4$, leading to the generating cubic $x_{n/4}^3 - 3x_{n/4} = 0$. In this case, the *altan*-[n]annulene spectrum contains a doubly-degenerate level at $x_{n/4} = 0$, and two doubly degenerate levels at $x_{n/4} = \pm\sqrt{3}$. It follows that every [$4N$]annulene generates an *altan*-[$4N$]annulene with at least three non-bonding molecular orbitals (a general proof that altanisation leads to increase by one the number of null eigenvalues of the adjacency matrix can be found in ref.[27], which can be considered an addition to the previously known cases of nullity of graphs[53]).
4. As the cubic can be written as $(x-\alpha_1)(x-\alpha_2)(x-\alpha_3) = 0$ in terms of its roots α_1, α_2 and α_3, it follows, by comparison with Eq. 5, that $\varepsilon_q(\varepsilon_q + 2) = -\alpha_1\alpha_2\alpha_3$ and $\varepsilon_q = \alpha_1 + \alpha_2 + \alpha_3$. The bonding orbitals of the parent annulene (positive eigenvalues) thus produce three roots such that $\alpha_1\alpha_2\alpha_3 < 0$ and $\alpha_1 + \alpha_2 + \alpha_3 > 0$, that is: two positive roots and one negative. This implies that each bonding q shell of the parent annulene generates two bonding and one antibonding shell in the *altan*-[n]annulene.
5. The same reasoning can be used to show that the antibonding orbitals of the parent [n]annulene produce two antibonding and one bonding copies in the *altan*-[n]annulene spectrum. One of the copies of the antibonding stack of orbitals in the *altan*-[n]annulene spectrum to be *reversed* with respect to the original, meaning that q for the hub will not increase regularly with energy of the orbitals of the derived *altan*.

3.1 *altan*-[$4N+2$]annulenes

From point 4, it follows that the $n/2$ bonding orbitals of an [n]annulene with n=$4N$+2 give rise to n bonding orbitals in the *altan*-[n]annulene. The remaining $n/2$ bonding orbitals of the *altan*-[n]annulene are generated from the antibonding orbitals of the parent annulene. Since any *altan*-[n]annulene has $3n$ π-electrons, it follows that *altan*-[n]annulenes with $n = 4N+2$ have all bonding levels completely filled.[36] Also, from point 2 we know that the LUMO of an *altan*-[n]annulene generated by a [$4N$+2]annulene is non-bonding, with $n/2$ angular nodes on the rim. From straightforward calculation of the roots of the cubic for [$4N+2$] annulenes, exemplified in Fig. 4 for *altan*-[10]annulene, we can also infer that (i) The two groups of bonding copies of the [n]annulene bonding orbitals can be described as in- and out-of-phase combinations of rim and hub orbitals with ring quantum numbers q and $q' = q$. Within these groups, ordering by q is pre-

served. The set of antibonding copies of the [n]annulene bonding orbitals arise from out-of-phase combination of hub and rim orbitals with ring quantum numbers q and $q' = n - q$. Within this set the q-ordering is reversed.

(ii) The two sets of antibonding descendants of the [n]annulene antibonding orbitals can be described as in- and out-of-phase combinations of rim and hub orbitals with ring quantum numbers q and $q' = n - q$. Within the out-of-phase set q-ordering is preserved, while it is reversed in the in-phase group. The set of bonding copies of the [n]annulene antibonding orbitals are in-phase combinations of hub and rim orbitals with ring quantum number q and $q' = q$. Within this set, the ordering by q is preserved. The three bonding frontier orbitals of the systems are $(\frac{n}{2} + \frac{n}{2}) \equiv ((2N+1)+(2N+1))$ and the pair $(\frac{n-2}{4} - \frac{n-2}{4}) \equiv (N-N)$, i.e (5+5) and (2-2) for the example in Fig. 4. These orbitals are close in energy, and their order changes with n: the non-degenerate orbital is the HOMO for $n = 6$ and $n = 10$, but has a lower energy than the pair for $n \geq 14$ ($N \geq 3$).

As already observed, the LUMO of the system is always the non-bonding orbital with HANC label $(\varnothing \frac{n}{2}) \equiv (\varnothing\ 2N+1)$. The LUMO has therefore the same $\mathrm{HANC_{rim}}$ as one bonding frontier orbital. Hence, the bonding-to-non-bonding transition (HOMO→LUMO transition for smaller annulenes, HOMO−1→LUMO transition for higher annulenes) gives rise to a strong paratropic ring-current on the rim.

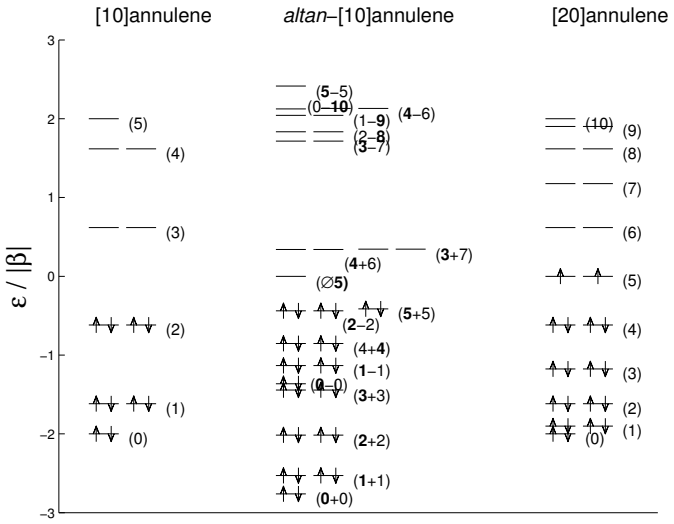

Fig. 4 Solutions of cubic equation (5) with azimuthal node-count labelling $\mathrm{HANC_{hub}} \pm \mathrm{HANC_{rim}}$ for *altan*-[10]annulene. Spectra of [10]annulene and [20]annulene are also shown for comparison. To keep track of the weights of the annulenic orbitals in the linear combination, HANC values are given in bold for annulenic orbitals with a population higher than 0.1. In case of null contribution of orbitals of an annulene (weight smaller than $1{\cdot}10^{-4}$), the ∅ sign is used.

Among the lowest lying antibonding orbitals of the *altan*-[n]annulene (LUMO+1 for n=6, LUMO+3 for higher annulenes) there is always a copy of the LUMO of the parent annulene, with label $(\frac{n+2}{4} + \frac{3n-2}{4}) \equiv ((N+1)+(3N+1))$, *i.e.*, a frontier orbital whose $\mathrm{HANC_{hub}}$ is one unit larger than the HOMO/HOMO−1 discussed above. It follows that in *altan*-[n]annulene, with $n = 4N+2$, the second strongest transition is purely diatropic and produces current that concentrates on the hub.

3.2 *altan*-[4N]annulenes

For *altan*-[4N]annulenes (Fig. 5), the same considerations apply: the parent bonding stack of levels produces two bonding copies that preserve q ordering and one reversed antibonding copy; the parent antibonding stack of levels produces one bonding copy with the same q-order, and two antibonding copies, the lower in energy having the reverse q-order. However, in equilateral parent [4N]annulenes the bonding and antibonding energy level stacks touch at the doubly degenerate non-bonding level. We have already seen from point 3 that, in fact, a [4N]annulene generates two additional zeros in the *altan*-[4N]annulene spectrum corresponding to $q = n/4 = N$, to give a total of three non-bonding levels. For a small distortion of the geometry (Jahn-Teller instability), the zero resulting from the non-bonding orbital described in point 2 will remain antibonding, but a gap opens up in the $q = n/4 = N$ doubly degenerate level. This implies that the $3n$ π-electrons of the *altan*-[n]annulene will occupy the n (bonding for a Jahn-Teller distorted system) levels generated by the $n/2$ bonding stack of the parent annulene, and the $n/2$ (bonding) levels generated by the $n/2$ antibonding stack of the parent annulene. This leads to frontier orbitals with a well-defined q character. The HOMO of the *altan*-[4N]annulene is always given by the

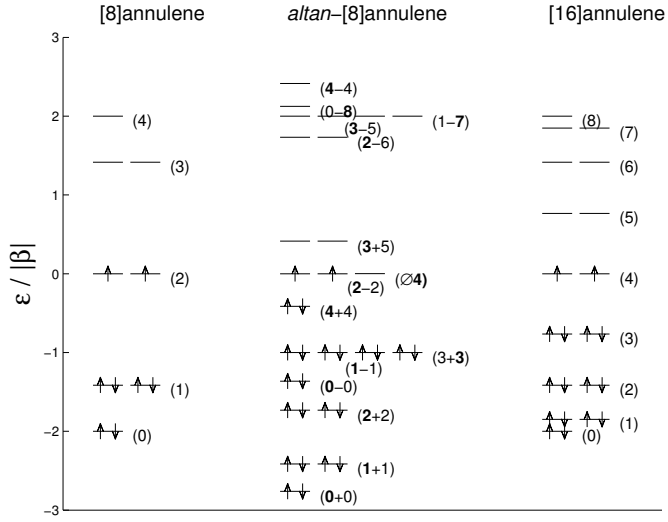

Fig. 5 Solutions of cubic equation (5) with azimuthal node-count labelling for *altan*-[8]annulene. Spectra of [8]annulene and [16]annulene are also shown for comparison. The degenerate (**2**-2) pair will be Jahn-Teller split, and thus generate a doubly occupied HOMO and the LUMO+1. Details of the labelling as in Fig. 4.

Jahn-Teller split rotational partner and derives essentially from the HOMO of the [4N]annulene; it has $\mathrm{HANC_{rim}} = \frac{n}{4} \equiv N$. As in the case of the large [4N+2] annulenes, the HOMO−1 of the

altan-[n]annulene is generated by the top antibonding level of the parent annulene, and has HANC label $(\frac{n}{2}-\frac{n}{2}) \equiv (2N-2N)$. The LUMO of the system, again as for the [$4N$+2] parent-annulene, is always given by the non-bonding orbital concentrated on the rim of the system, and has HANC label $(\varnothing\frac{n}{2}) \equiv (\varnothing 2N)$. Finally, the LUMO+1 of the *altan*-[$4N$]annulene is given by the antibonding component of the Jahn-Teller split rotational partner, and hence has HANC=$\frac{n}{4} \equiv N$. It follows that the two dominant transitions characterizing the ring-current response of any *altan*-[$4N$]annulene arise from

1) HOMO$-1 \rightarrow$LUMO (paratropic on the rim, as in [$4N$+2]parent annulenes)

2) HOMO $\rightarrow$LUMO+1 (paratropic on the hub).

3.3 *altan*-[$4N+1$]annulenes

The parent annulenes have $2N+1$ bonding orbitals and $2N$ antibonding orbitals. Since the cubic (5) always produces two bonding copies of the bonding level, and one bonding copy of the antibonding stack, the generated *altan*-[$4N$+1]annulene graph will have $2(2N+1)+2N = 6N+2$ bonding orbitals. The typical spectrum is shown in Fig. 6 for *altan*-[9]annulene.

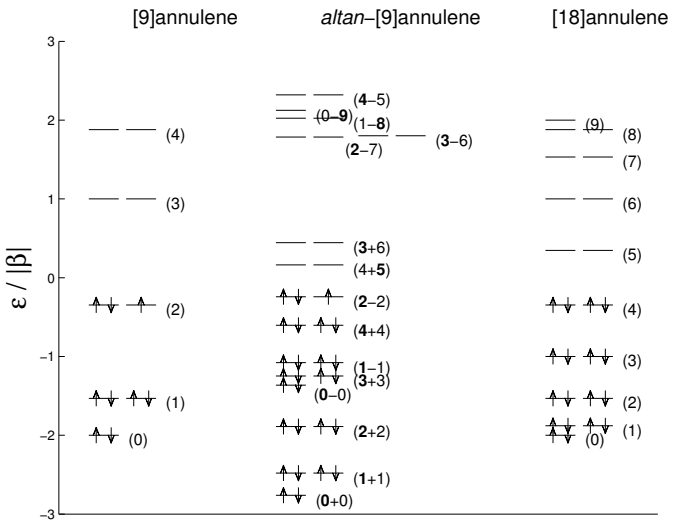

Fig. 6 Solutions of cubic equation 5 with azimuthal node-count labelling for *altan*-[9]annulene. The spectra of the parent annulenes are also shown. Details of the labelling as in Fig. 4.

3.3.1 Monoanion

The *altan*-[$4N$+1]annulene graphs have $3n = 3(4N+1) = 12N+3$ vertices, so that the anions have $12N+4$ electrons. From the cubic, we know that there are exactly $6N+2$ bonding orbitals, so that the monoanions *altan*-[$4N$+1]annulenes$^-$ are properly closed-shell (as are the anions of the parent [$4N$+1]annulenes).

3.3.2 Monocation

The *altan*-[n]annulene graph has $3n = 3(4N+1)$ vertices, so that the cation has $12N+2$ electrons. Hence, from the cubic, we know that there are exactly $6N+2$ bonding orbitals with a HOMO that is doubly degenerate deriving from the $q = n$ orbital of the parent annulene. It follows that the cation is an open-shell system. A Jahn-Teller distortion would lower the symmetry and open a gap between the two components of the doubly-degenerate HOMO, so that a new paratropic transition concentrated on the hub would arise between the new non-degenerate HOMO with $q = n$, and the new LUMO with $q = n$. Note that the diatropic ring current on the rim is expected to survive, in this case generated by the HOMO-1/HOMO-2 to LUMO+1/LUMO+2 translational transition discussed in the previous paragraph (see Fig. 6).

3.4 *altan*-[$4N+3$]annulenes

The parent annulenes have $2N+1$ bonding orbitals and $2N+2$ antibonding orbitals. As the cubic 5 always produces two bonding copies of the parent annulene bonding level, and one bonding copy of the parent antibonding stack, the generated *altan*-[$4N+3$]annulene graph will have $2(2N+1)+2N+2 = 6N+4$ bonding orbitals (Fig. 7).

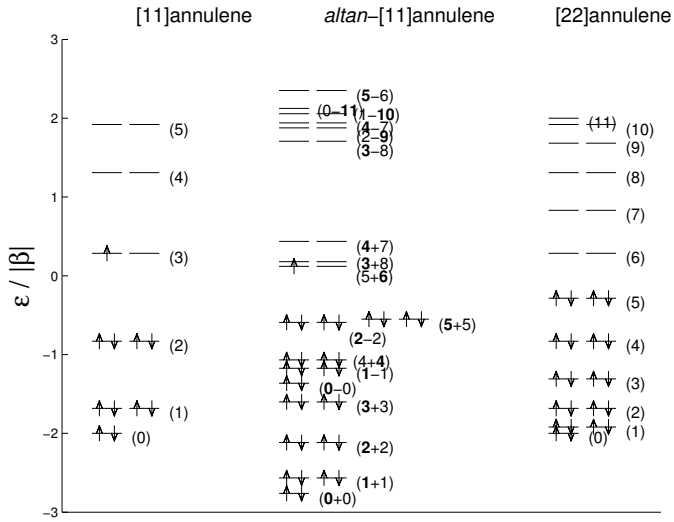

Fig. 7 Solutions of cubic equation (5) with azimuthal node-count labelling for *altan*-[11]annulene. Spectra of the parent annulenes are also shown. Details of the labelling as in Fig. 4.

3.4.1 Monocation

The graphs of *altan*-[$4N+3$]annulenes have $3n = 3(4N+3)$ vertices, so that the cations have $12N+8$ electrons. From the cubic we know that there are exactly $6N+4$ bonding orbitals, so that *altan*-[$4N+3$]annulenes$^+$ are properly closed-shell (as are the parent [$4N+3$]annulenes$^+$). From the HANC values of the eigenvalues of *altan*-[11]annulene (Fig. 7), the current-density pattern can be expected to have a diatropic hub (HOMO-2/HOMO-3 $\rightarrow$ LUMO+2/LUMO+3 transition) and a diatropic rim (HOMO/HOMO-1 $\rightarrow$ LUMO/LUMO+1 transition).

3.4.2 Monoanion

A degenerate level is occupied by two electrons and a closed-shell configuration can form upon Jahn-Teller splitting. In the case of *altan*-[11]annulene the HOMO and LUMO would have HANC labels (5+**6**) and the HOMO→LUMO transition should be associated with a strong paratropic circulation on the rim, counterbalanced by a diatropic circulation stemming from the HOMO−1/HOMO−2→LUMO transition (for the use of bold fonts for HANCs see the caption of Fig. 4). The hub can be expected to support a paratropic current arising from the HOMO→ LUMO transition, counterbalanced by a diatropic current arising from the HOMO−3/HOMO−4→LUMO+1/LUMO+2 transition. It has to be noted that upon binding to the rim, the degenerate pair on the hub with HANC=3 splits in order to give the (**3**+8) and (**3**+3) pairs, which are not the frontier orbitals.

4 Ab Initio Calculations

4.1 Computational Methods

Geometries and unperturbed Kohn-Sham orbitals were obtained using the B97-2 functional,[54] which gives geometries comparable to B3LYP, but shielding constants superior to those obtained by B3LYP and other functionals.[55] The 6-31G(*d*,*p*) basis set was adopted throughout. Geometries were determined at the restricted level, and stability of the wavefunction checked using the `Stable` function of Gaussian 09.[56] Where UHF instability was detected, geometries and currents were recomputed at the unrestricted level, and in these cases, the character of the wavefunction was further investigated through CAS(n,m)SCF calculations, where the usual notation is used to indicate that n electrons are distributed in all possible ways in m active orbitals.[57] A (2,2) active space was initially chosen according to the UNO-CAS method.[58] Tests with larger active spaces, (4,4) and (6,6) were then performed. The chosen active spaces led to smooth non-oscillating convergence.

Rather than the natural orbital occupation numbers, we will mainly report the poly-radical character $y_i = \frac{1}{2}(n^{\rm odd}_{{\rm HONO}-i} + n^{\rm odd}_{{\rm LUNO}+i})$, where the $n^{\rm odd}_{\rm HONO}$ and $n^{\rm odd}_{\rm LUNO}$ are the absolute values of the differences between the occupation numbers of the natural and canonical orbitals for the highest occupied and the lowest unoccupied orbital, respectively.[59] A value of y_0 close to 1 is indicative of a well-defined diradical character. Values of y_1, y_2,... close to 1 are indicative of significant tetraradical, hexaradical... character.

Equalization of bond length is often considered a criterion of aromaticity.[60] Rather than use one of the indicators proposed,[60,61] which may have problems for rings with odd number of bonds,[62] we will report simple arithmetic averages $\overline{R}$ and unbiased coefficient of variations, which for samples of size n_b bond lengths can be computed as $V^* = (1+\frac{1}{4n_b})s(R)/\overline{R}\times 100$, where $s(R)$ is the sample standard deviation of the bond lengths.[63]

For closed-shell systems, current-density was computed at the B97-2/6-31G(*d*,*p*) level with the CTOCD-DZ2 method, using SYSMO[64]. For the open-shell molecules the first-order density matrices perturbed by an external magnetic field, and the associated CTOCD-DZ2 current-density vector fields, were computed at the B97-2/6-31G(d,p) level using an open-shell version[51,65–67] of SYSMO, where the coupled-perturbed calculations were started from unperturbed Kohn-Sham orbitals converged with Gaussian 09 at the same level of theory. Sketches of the current are obtained using a surface placed 1 au above the molecule. For consistency with previous work,[5,6] the probability current density[68] is plotted, so that paratropic/diatropic circulations run in clockwise/anti-clockwise sense for a magnetic field pointing out of the page. More details on the plots can be found in the caption of Fig. 9.

4.2 Geometries and Nature of Ground States

Table 1 reports information on the optimized geometries. The only planar molecules turn out to be *altan*-[10]annulene and *altan*-[11]annulene$^{\pm1}$; all others have a bowl shape, with the exception of *altan*-[12]annulene which resembles a twisted doughnut. All structures are local minima.

As a first remark, we note that for all molecules the spokes are long bonds, which is consistent with the decoupling expected in altanisation. With the single exception of *altan*-[9]annulene^{+1}, spokes are on average longer than the reference sp^2-sp^2 single bond: 1.478 ± 0.012Å.[69]

For comparison, the spokes of the two synthesized altans, 8MC and 10MC, are shorter, in the range 1.453-1.463 Å. Restricted calculations show the expected behavior for rims and hubs in neutral systems: $4N$ loops show bond-length variation ($V^*>0$), while $4N+2$ loops show equalization ($V^*=0$). Bond-length equalization is also observed for $4N+2$ ionic *altans*, while for $4N$ ionic *altans* some variation is present not only on the hub, but also on the rim.

Use of the unrestricted optimization in the four molecules affected by UHF instability led to minor changes in the case of *altan*-[12]annulene alone, where the equilibrium geometry lies on a very shallow hypersurface (the lowest vibrational frequency, representing an overall puckering, is only 6.2 and 1.7 cm^{-1} at restricted and unrestricted levels, respectively). The two geometries are indistinguishable if an ultrafine grid is used for computing integrals. For the other three molecules affected by UHF instability, the unrestricted optimization led to a complete equalization of bond lengths and increased symmetry (from C_4 to C_8 for *altan*-[8]annulene, and from C_1 to C_{9v} for *altan*-[9]annulene$^+$). Owing to the open-shell nature of the systems, these changes cannot be straightforwardly considered as aromatisation processes. Indeed, singlet D_{4h} cyclobutadiene is endowed with a strong paratropic current,[70] and the same is expected for D_{8h} cyclooctatetraene,[71,72] whereas the opposite behavior characterizes triplet states.[35]. The UB97-2 solution has high spin contamination: in all cases $S(S+1)\simeq 1$ and only two natural orbital occupation numbers are different from closed-shell values, both taking the value 1.0.

The nature of the ground states was checked at the more accurate CASSCF level. The differences $\Delta_{\rm ST} = E_{\rm T} - E_{\rm S}$ between the energy of the lowest triplet $E_{\rm T}$ and singlet $E_{\rm S}$ state calculated at CASSCF level are reported in Table 2, together with

Table 1 Geometrical features of the molecules studied: point group, averages (in Å), standard deviations (in Å) and coefficient of variation of bond-lengths in hub, rim and spokes (in Å). Geometrical optimization at RB97-2 level (and UB97-2 where the point group is preceded by a U) in the 6-31G(d,p) basis set.

Molecule	PG		R_{av}	$s(R)$	V*
altan-[8]annulene	C_4	hub	1.393	0.050	3.68
		rim	1.426	0.047	3.36
		spokes	1.474	0.001	0.06
	U C_8	hub	1.391	0.000	0.00
		rim	1.426	0.047	3.38
		spokes	1.473	0.000	0.00
altan-[9]annulene^{+1}	C_1	hub	1.388	0.032	2.38
		rim	1.420	0.004	0.29
		spokes	1.467	0.004	0.31
	U C_{9v}	hub	1.387	0.000	0.02
		rim	1.421	0.001	0.06
		spokes	1.466	0.002	0.13
altan-[9]annulene^{-1}	C_{9v}	hub	1.386	0.000	0.00
		rim	1.424	0.000	0.00
		spokes	1.486	0.000	0.00
altan-[10]annulene	C_{10h}	hub	1.380	0.000	0.00
		rim	1.425	0.043	3.03
		spokes	1.486	0.000	0.00
altan-[11]annulene^{+1}	D_{11h}	hub	1.403	0.000	0.00
		rim	1.399	0.000	0.00
		spokes	1.490	0.000	0.01
altan-[11]annulene^{-1}	C_{2v}	hub	1.410	0.025	1.82
		rim	1.402	0.021	1.53
		spokes	1.492	0.028	1.94
	U C_{2v}	hub	1.410	0.021	1.49
		rim	1.402	0.013	0.94
		spokes	1.492	0.008	0.55
altan-[12]annulene	C_2	hub	1.423	0.047	3.34
		rim	1.392	0.031	2.22
		spokes	1.504	0.000	0.03

Table 2 Indices of polyradical character, y_0 and y_1, for the lowest energy singlet (S) and triplet (T) states of *altan*-[8]annulene (a8a), *altan*-[9]annulene$^+$ (a9a+), *altan*-[11]annulene$^-$ (a11a-) and *altan*-[12]annulene (a12a) at different CAS(n,m)SCF levels, in with the 6-31G(d,p) basis set. Δ_{ST} is the energy difference in eV. Indices y_0 and y_1 are derived from the populations of natural orbitals.[59]

	(n,m)	y_0^S	y_1^S	y_0^T	y_1^T	Δ_{ST}
a8a	(2,2)	0.11	-	1	-	0.50
a8a	(4,4)	0.13	0.10	1.00	0.07	0.59
a9a+	(2,2)	0.11	-	1.00	-	0.39
a9a+	(4,4)	0.15	0.07	1.00	0.06	0.59
a9a+	(6,6)	0.18	0.95	1.00	0.07	0.44
a11a−	(2,2)	0.40	-	1.00	-	−0.11
a11a−	(4,4)	0.96	0.08	0.97	0.00	−0.10
a11a−	(6,6)	0.81	0.08	1.00	0.08	0.00_6
a12a	(2,2)	0.00_2	-	1.00	-	1.88
a12a	(4,4)	0.00	0.00	1.00	0.00	1.33

their polyradical characters. All the molecules are predicted to have singlet ground states in their symmetrized geometries. The ST gap Δ_{ST} is larger than 1 eV for *altan*-[12]annulene, close to 0.5 eV for *altan*-[8]annulene and *altan*-[9]annulene$^+$ and vanishingly small for *altan*-[11]annulene$^-$. Consistently, the diradical character y_0^S is practically null for *altan*-[12]annulene, small for *altan*-[8]annulene and *altan*-[9]annulene^{+1}, and close to 1 for *altan*-[11]annulene$^-$.

4.3 Current Density Patterns

4.3.1 Neutral systems

The current density maps computed at the restricted level for the three neutral systems show what could be expected for disjoint annulenes: diatropic or paratropic for $4N+2$ or $4N$ annulenes, in full agreement with the altanisation design strategy.[5,6] For the sake of completeness, the maps for *altan*-[10]annulene and *altan*-[12]annulene are shown in Fig. 8. However, *altan*-[8]annulene is affected by a UHF instability. The unrestricted calculation for *altan*-[8]annulene is qualitatively similar to the restricted calculation (Fig. 9). The absence of any qualitative change in the pattern

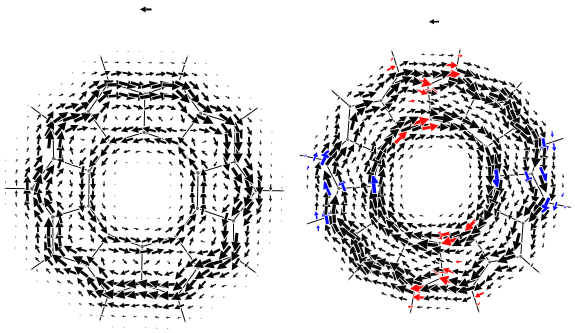

Fig. 8 Maps of probability-current density for *altan*-[10]annulene and (left) *altan*-[12]annulene (right) computed at the B97-2/6-31G(*d*,*p*)//B97-2/6-31G(*d*,*p*). The maps are computed on a surface placed at a height of 1 bohr above the molecule. For the bowl-shaped molecule on the left, the point of view is outside the bowl and far away. The isolated arrow in each panel indicates the maximum value of the current density in benzene computed at the same level ($j_{max} = 0.07$ au). For a magnetic field pointing to the viewer, a diatropic/paratropic probability current density is anticlockwise/clockwise. Red/blue arrows indicate a current density vector with a nonclassical component parallel/antiparallel to the magnetic field that exceeds 10%.

is consistent with the small diradical character reported in Table 1.

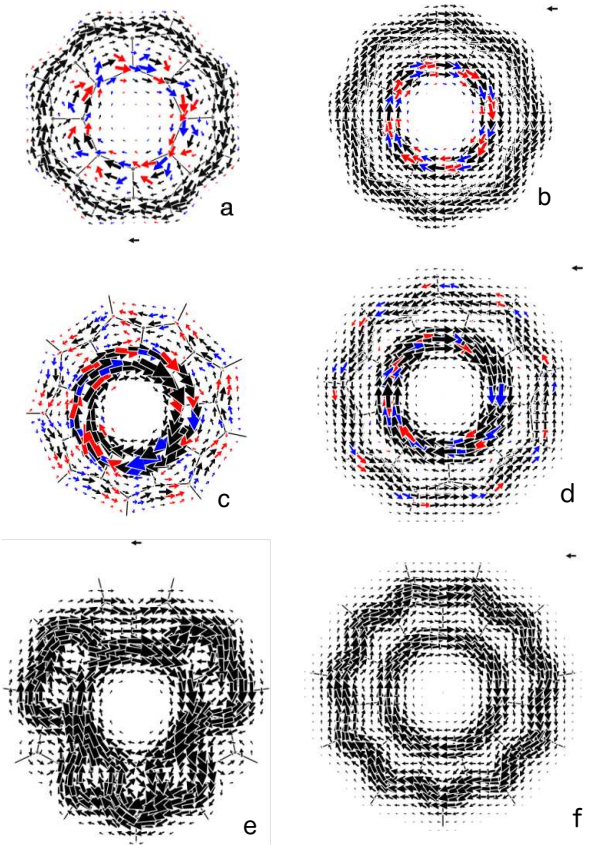

Fig. 9 Maps of the probability current density of π electrons computed at the B97-2/6-31G(*d*,*p*)//B97-2/6-31G(*d*,*p*) level (left) and UB97-2/6-31G(*d*,*p*)//UB97-2/6-31G(*d*,*p*) levels (right) for *altan*-[8]annulene (a,b), *altan*-[9]annulene^{+} (c,d), and *altan*-[11]annulene^{-} (e,f) computed on a surface placed at a height of 1 bohr above the molecule. For bowl-shaped molecules (a-d), the point of view is outside the bowl and far away. Other plotting details as in Figure 8.

4.3.2 $(4N+2)\pi$ *altan* ions

The current-density map of *altan*-[9]annulene^{-1} and *altan*-[11]annulene^{+1} show two strong concentric diatropic circulations, as expected from the Hückel scheme above (Fig. 10).

4.3.3 $4N\pi$ *altan* ions

At the restricted level, the current density map of *altan*-[9]annulene^{+} shows a a strong paratropic hub inside a diatropic rim, consistently with the Hückel analysis above, and with a prediction of full decoupling of a charged annulene inside a $4N+2$ annulene. The symmetrization occurring at the unrestricted level does not affect the overall tropicity, which remains diatropic on the rim and paratropic on the hub.

For *altan*-[11]annulene^{-1} the current density maps at both restricted and unrestricted level show a global paratropic response, and the diatropic rim is absent. As with the geometry, the map obtained at the unrestricted level is noticeably more symmetric. Interestingly, the pattern could also not be anticipated considering only resonance structures with fixed single bonds on the spokes; it *requires* significant participation of resonance structures such as II in Fig. 2.

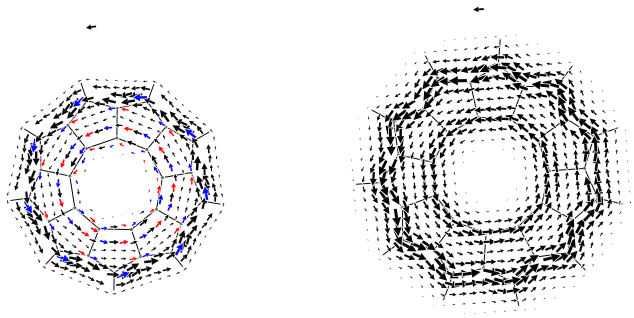

Fig. 10 Maps of the probability current density of π electrons of *altan*-[9]annulene^{-1} and *altan*-[11]annulene^{+1}. Details of the maps as in Fig. 8.

5 Conclusions

The altanisation strategy was introduced to design large paratropic circulations,[22,26] of interest for application in organic electronic devices.[1,2,4] Here we have considered altanisation of [*n*]annulenes, extending previous investigations[5,6] to anions and cations of *altans* of odd-membered [*n*]annulenes.

Analytical expressions for the eigenvalues of the Hückel Hamiltonian for *altan*-[*n*]annulenes have been derived and used to predict the tropicities of the concentric rings of atoms. Finally, density-functional calculations have been performed on seven *altan*-[*n*]annulenes, three neutral and four charged. In presence of instability of the closed-shell singlet wavefunction, its diradical character has been studied by CAS calculations.

For neutral systems, already discussed as prototypal altan systems,[18] there is at most a mild diradical character, and the tropicities are in wide agreement with what could be expected for two decoupled annulenes. The charged systems always have a $4N+2$ perimeter and thus, in the annulene-within-an-annulene framework, should all display a diatropic perimeter. The anion *altan*-[11]annulene^{-} is a notable exception among the molecules studied: its current-density map shows two concentric paratropic circulations. A first interpretation of this different behavior can be obtained considering resonance structures such as II in Scheme 2, which are characterized by $4N$ conjugated circuits.

Also within the ipsocentric approach, even operated at the tight binding level, the paratropic circulation on the hub is understandable, because the frontier orbitals do not stem from the degenerate frontier orbitals of the [11]annulene^{-} fragment.

It is noteworthy that the only *altan*-molecule studied here that does not conform to the AWA scheme has a well-defined diradical character in its singlet ground state (Table 2). From the perspective of resonance structures, it can be noted that just as the onset of a single charge in an *altan*-molecule allows resonance forms where the spokes are not single bonds, the presence of two or more unpaired electrons, as needed to describe open-shell diradicals and polyradicals, also allows double bond character of the

spokes and thus hints at a stronger coupling of the perimeter and the inner part of the *altan*-molecule.

From the perspective of Hückel molecular orbitals, an uncoupled *altan*-[11]annulene$^-$ has 4 degenerate orbitals, labeled (3) on the hub and (6) on the rim, Fig. 7. As these orbitals have no overlap, an open-shell singlet is well understandable, and can be described as an [11]annulene radical within a [22]annulene anion. Both annulenes can then be straightforwardly predicted to host a paratropic current. We can anticipate that the altanisation strategy will be in difficulties whenever the altan will be an open-shell singlet, because of an incorrect identification of the parent units. However, proper identification of the multiplicity of the parent units will reconcile the counting of carbon atoms with the global tropicities. This extension of the altanisation strategy could be beneficial for the quest of new materials, also considering that, thanks to the choice of a non-all-*cis* conformation of the parent annulene, more *altan*-annulenes are likely to become available experimentally in the future.[32]

Conflicts of interest

There are no conflicts to declare.

Acknowledgments

Financial support from MIUR is gratefully acknowledged.
AS acknowledges support from an Australian Research Council Discovery Project Grant DP170100034.

Notes and references

1 Y. Sun, Y. Guo and Y. Liu, *Mater. Sci. Eng. R Rep.*, 2019, **136**, 13–26.
2 T. Nishinaga, T. Ohmae, K. Aita, M. Takase, M. Iyoda, T. Arai and Y. Kunugi, *Chem. Commun.*, 2013, **49**, 5354.
3 J. Cao, G. London, O. Dumele, M. von Wantoch Rekowski, N. Trapp, L. Ruhlmann, C. Boudon, A. Stanger and F. Diederich, *J. Am. Chem. Soc.*, 2015, **137**, 7178–7188.
4 J. Liu, J. Ma, K. Zhang, P. Ravat, P. Machata, S. M. Avdoshenko, F. Hennersdorf, H. Komber, W. Pisula, J. J. Weigand, A. A. Popov, R. Berger, K. Müllen and X. Feng, *J. Am. Chem. Soc.*, 2017, **139**, 7513–7521.
5 G. Monaco, R. G. Viglione, R. Zanasi and P. W. Fowler, *J. Phys. Chem. A*, 2006, **110**, 7447–7452.
6 G. Monaco, P. Fowler, M. Lillington and R. Zanasi, *Angew. Chem., Int. Ed.*, 2007, **46**, 1889–1892.
7 W. E. Barth and R. G. Lawton, *J. Am. Chem. Soc.*, 1966, **88**, 380–381.
8 M. Baumgarten, L. Gherghel, M. Wagner, A. Weitz, M. Rabinovitz, P.-C. Cheng and L. T. Scott, *J. Am. Chem. Soc.*, 1995, **117**, 6254–6257.
9 G. Ege and H. Vogler, *Theor. Chim. Acta*, 1972, **26**, 55–65.
10 E. Steiner, P. W. Fowler and L. W. Jenneskens, *Angew. Chem. Int. Ed.*, 2001, **40**, 362–366.
11 A. Acocella, R. Havenith, E. Steiner, P. Fowler and L. Jenneskens, *Chem. Phys. Lett.*, 2002, **363**, 64–72.
12 J.-i. Aihara, *Chem. Phys. Lett.*, 2004, **393**, 7–11.
13 T. K. Dickens and R. B. Mallion, *J. Phys. Chem. A*, 2011, **115**, 351–356.
14 T. K. Dickens, J. A. N. F. Gomes and R. B. Mallion, *J. Chem. Theory Comput.*, 2011, **7**, 3661–3674.
15 T. K. Dickens and R. B. Mallion, *Phys. Chem. Chem. Phys.*, 2013, **15**, 8245.
16 J. Aihara, *RSC Adv.*, 2014, **4**, 7256.
17 G. Monaco and R. Zanasi, *J. Chem. Phys.*, 2009, **131**, 044126–044126.
18 G. Monaco, M. Memoli and R. Zanasi, *J. Phys. Org. Chem.*, 2013, **26**, 109–114.
19 E. Steiner and P. W. Fowler, *J. Phys. Chem. A*, 2001, **105**, 9553–9562.
20 E. Steiner and P. W. Fowler, *Chem. Commun.*, 2001, 2220–2221.
21 J. A. Pople and K. Untch, *J. Am. Chem. Soc.*, 1966, **88**, 4811–4815.
22 G. Monaco and R. Zanasi, *J. Phys. Chem. A*, 2012, **116**, 9020–9026.
23 T. K. Dickens and R. B. Mallion, *J. Phys. Chem. A*, 2014, **118**, 3688–3697.
24 I. Gutman, *J. Serb. Chem. Soc.*, 2014, **79**, 1515–1521.
25 T. K. Dickens and R. B. Mallion, *Chem. Commun.*, 2015, **51**, 1819–1822.
26 R. Zanasi, P. Della Porta and G. Monaco, *J. Phys. Org. Chem.*, 2016, **29**, 793–798.
27 I. Gutman, *Iranian J. Math. Chem.*, 2014, **5**, 85–90.
28 G. Monaco, *Phys. Chem. Chem. Phys.*, 2015, **17**, 28544–28547.
29 T. K. Dickens and R. B. Mallion, *J. Phys. Chem. A*, 2015, **119**, 5019–5025.
30 M. Nakano, *Excitation Energies and Properties of Open-Shell Singlet Molecules*, Springer International Publishing, Cham, 2014.
31 C. Liu, M. E. Sandoval-Salinas, Y. Hong, T. Y. Gopalakrishna, H. Phan, N. Aratani, T. S. Herng, J. Ding, H. Yamada, D. Kim, D. Casanova and J. Wu, *Chem*, 2018, **4**, 1586–1595.
32 C. Liu, Y. Ni, X. Lu, G. Li and J. Wu, *Acc. Chem. Res.*, 2019, **52**, 2309–2321.
33 *Pure Appl. Chem.*, 1981, **53**, 733–752.
34 N. C. Baird, *J. Am. Chem. Soc.*, 1972, **94**, 4941–4948.
35 V. Gogonea, P. von Ragué Schleyer and P. R. Schreiner, *Angew. Chem. Int. Ed.*, 1998, **37**, 1945–1948.
36 D. A. Bochvar, E. G. Gal'pern, and N. P. Gambaryan, *Izv. Akad. Nauk SSSR, Ser. Khim.* 1970, **3**, 435–437.
37 M. Randić, *Chem. Rev.*, 2003, **103**, 3449–3606.
38 M. Randić, *Chem. Phys. Lett.*, 2010, **500**, 123–127.
39 T. A. Keith and R. F. W. Bader, *J. Chem. Phys.*, 1993, **99**, 3669.
40 T. A. Keith and R. F. Bader, *Chem. Phys. Lett.*, 1993, **210**, 223–231.
41 P. Lazzeretti, M. Malagoli and R. Zanasi, *Chem. Phys. Lett.*, 1994, **220**, 299–304.
42 E. Steiner, A. Soncini and P. W. Fowler, *J. Phys. Chem. A*, 2006, **110**, 12882–12886.

43 P. W. Fowler, E. Steiner, R. W. A. Havenith and L. W. Jenneskens, *Magn. Reson. Chem.*, 2004, **42**, S68–S78.

44 G. Monaco, L. T. Scott and R. Zanasi, *J. Phys. Chem. A*, 2008, **112**, 8136–8147.

45 T. K. Dickens and R. B. Mallion, *MATCH Commun. Math. Comput. Chem.*, 2016, **76**, 297–356.

46 J. R. Platt, *J. Chem. Phys.*, 1949, **17**, 484.

47 M. Damnjanović, I. Božović and N. Božović, *J. Phys. A*, 1983, **16**, 3937–3947.

48 M. Damnjanović, I. Milošević, T. Vuković and R. Sredanović, *Phys. Rev. B*, 1999, **60**, 2728–2739.

49 B. M. Peden, R. Bhat, M. Krï£imer and M. J. Holland, *J. Phys. B: At., Mol. Opt. Phys.*, 2007, **40**, 3725–3744.

50 A. Soncini, C. Domene, J. Engelberts, P. Fowler, A. Rassat, J. van Lenthe, R. Havenith and L. Jenneskens, *Chem.-Eur. J.*, 2005, **11**, 1257–1266.

51 A. Soncini and P. Fowler, *Chem. Phys. Lett.*, 2008, **450**, 431–436.

52 G. Monaco and R. Zanasi, *Int. J. Quantum Chem.*, 2009, **109**, 243–249.

53 I. Gutman and B. Borovićanin, *Zbornik Radova*, 2011, 137–154.

54 P. J. Wilson, T. J. Bradley and D. J. Tozer, *J. Chem. Phys.*, 2001, **115**, 9233.

55 D. Flaig, M. Maurer, M. Hanni, K. Braunger, L. Kick, M. Thubauville and C. Ochsenfeld, *J. Chem. Theory Comput.*, 2014, **10**, 572–578.

56 M. J. Frisch, G. W. Trucks, H. B. Schlegel, G. E. Scuseria, M. A. Robb, J. R. Cheeseman, G. Scalmani, V. Barone, B. Mennucci, G. A. Petersson, H. Nakatsuji, M. Caricato, X. Li, H. P. Hratchian, A. F. Izmaylov, J. Bloino, G. Zheng, J. L. Sonnenberg, M. Hada, M. Ehara, K. Toyota, R. Fukuda, J. Hasegawa, M. Ishida, T. Nakajima, Y. Honda, O. Kitao, H. Nakai, T. Vreven, J. A. Montgomery, Jr., J. E. Peralta, F. Ogliaro, M. Bearpark, J. J. Heyd, E. Brothers, K. N. Kudin, V. N. Staroverov, R. Kobayashi, J. Normand, K. Raghavachari, A. Rendell, J. C. Burant, S. S. Iyengar, J. Tomasi, M. Cossi, N. Rega, J. M. Millam, M. Klene, J. E. Knox, J. B. Cross, V. Bakken, C. Adamo, J. Jaramillo, R. Gomperts, R. E. Stratmann, O. Yazyev, A. J. Austin, R. Cammi, C. Pomelli, J. W. Ochterski, R. L. Martin, K. Morokuma, V. G. Zakrzewski, G. A. Voth, P. Salvador, J. J. Dannenberg, S. Dapprich, A. D. Daniels, Ö. Farkas, J. B. Foresman, J. V. Ortiz, J. Cioslowski and D. J. Fox, *Gaussian 09 Revision D.01*, Gaussian Inc. Wallingford CT 2009.

57 F. Jensen, *Introduction to Computational Chemistry*, Wiley, 2016.

58 J. M. Bofill and P. Pulay, *J. Chem. Phys.*, 1989, **90**, 3637–3646.

59 M. Nakano, H. Fukui, T. Minami, K. Yoneda, Y. Shigeta, R. Kishi, B. Champagne, E. Botek, T. Kubo, K. Ohta and K. Kamada, *Theor. Chem. Acc.*, 2011, **130**, 711–724.

60 T. M. Krygowski and M. K. Cyrański, *Chem. Rev.*, 2001, **101**, 1385–1420.

61 J. Kruszewski and T. Krygowski, *Tetrahedron Lett*, 1972, **13**, 3839–3842.

62 E. D. Raczyńska, M. Hallman, K. Kolczyńska and T. M. Stępniewski, *Symmetry*, 2010, **2**, 1485–1509.

63 R. R. Sokal and F. J. Rohlf, *Biometry: The Principles and Practices of Statistics in Biological Research*, W. H. Freeman, 1994.

64 P. Lazzeretti, M. Malagoli and R. Zanasi, *SYSMO Package*, Universities of Modena and Salerno.

65 A. Soncini, *J. Chem. Theory Comput.*, 2007, **3**, 2243–2257.

66 A. Soncini, A. M. Teale, T. Helgaker, F. De Proft and D. J. Tozer, *J. Chem. Phys.*, 2008, **129**, 074101.

67 A. Soncini and P. W. Fowler, *Chem.-Eur. J.*, 2013, **19**, 1740–1746.

68 P. Lazzeretti, *Handbook of Molecular Physics and Quantum Chemistry, 3 Volume Set*, John Wiley & Sons Inc, 2003, vol. 3, ch. 3, pp. 53–145.

69 F. H. Allen, D. G. Watson, L. Brammer, A. G. Orpen, R. Taylor in International Tables for Crystallography, Vol. C (Eds. A. J. C.Wilson, E. Princs), Kluwer, Dodrecht, 1999, p. 791.

70 S. Pathak, R. Bast and K. Ruud, *J. Chem. Theory Comput.*, 2013, **9**, 2189–2198.

71 P. B. Karadakov, *J. Phys. Chem. A*, 2008, **112**, 12707–12713.

72 T. Nishinaga, T. Ohmae and M. Iyoda, *Symmetry*, 2010, **2**, 76–97.